J|A|C|S
JOURNAL OF THE AMERICAN CHEMICAL SOCIETY

Article

Cite This: *J. Am. Chem. Soc.* 2017, 139, 18262−18270

pubs.acs.org/JACS

Downloaded via HEBREW UNIV OF JERUSALEM on December 18, 2018 at 12:48:10 (UTC).
See https://pubs.acs.org/sharingguidelines for options on how to legitimately share published articles.

Free Carrier Emergence and Onset of Electron−Phonon Coupling in Methylammonium Lead Halide Perovskite Films

Tufan Ghosh, Sigalit Aharon, Lioz Etgar, and Sanford Ruhman*

Institute of Chemistry, The Hebrew University of Jerusalem, Jerusalem, Israel 91904

Supporting Information

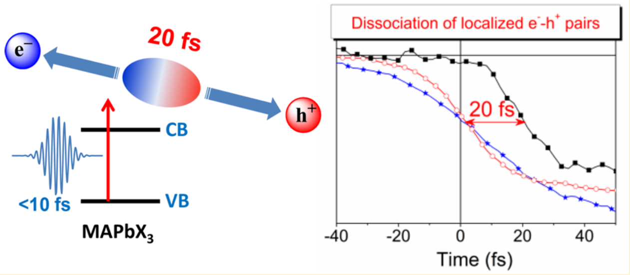

ABSTRACT: Sub-10 fs resolution pump−probe experiments on methylammonium lead halide perovskite films are described. Initial response to photoexcitation is assigned to localized hot excitons which dissociate to free carriers. This is attested to by band integrals of the pump−probe spectra where photoinduced bleaching rises abruptly 20 fs after photoexcitation. Later stages of spectral evolution are consistent with hot carrier cooling, during which state filling induced bleaching of interband and exciton transitions curiously more than doubles. Electron coupling to optical phonons is observed as periodic spectral modulations in the pump−probe data of both films. Fourier analysis identifies active phonons at ∼100 and 300 wavenumbers pertaining to the lead-halide framework and organic cation motions, respectively. Coupling strengths estimated from the depth of these modulations are in the weak coupling limit, in agreement with values extracted from temperature dependent emission line shape analysis. These findings support free carriers in these materials existing as large polarons. Accordingly, these modes are probably not dictating the moderate carrier mobility in this material.

INTRODUCTION

The impressive power conversion efficiency (∼20%) obtained in solar cells based on three-dimensional organic lead halide perovskites (OLHP), along with their ease of preparation, have generated an immense effort to understand the underlying photophysics. Results show that crucial factors behind their high power conversion efficiency are large optical absorption cross sections, substantial electron−hole diffusion lengths and slow electron−hole recombination rates.[1−10] Given OLHP's hybrid nature, assessing the roles of exciton vs free carrier transport has been an issue of central importance. While views on this vary, most studies highlight the essential role of free electrons and holes in the context of photovoltaic performance.[11,12] Under solar irradiation, most photons absorbed in methylammonium lead iodide perovskite (MAPbI$_3$) possess ∼0.4 eV of excess energy above the 1.65 eV band gap (BG). Accordingly characterizing the dynamics of free carrier generation and relaxation is of central importance, requiring ultrafast spectroscopic investigation.

A number of dynamic spectral features are common to femtosecond pump−probe studies on OLHP films: (1) a rapid buildup of intense photoinduced bleach (PIB) centered at the optical band-edge, which broadens with increasing pump fluence, (2) the appearance of a short-lived photoinduced absorption (PIA) band to the "red" of the optical band edge (BE), which decays over the course of hot carrier cooling, and (3) a slowly rising low intensity broad PIA near ∼650 nm.[13−20] Scenario (1) is often assigned to low energy state filling, and scenario (2) to shifting of exciton states due to band gap renormalization by hot carriers. These assignments are based on the dependence of these features on pump fluence and wavelength. Finally, several interpretations of the delayed broad PIA higher in the interband continuum have been suggested. Some have assigned this to the same band gap renormalization mentioned above, while others trace it to additional intraband excitations. All of these need to be re-examined in light of a recent study which assign this band to pump induced variations in reflectivity of the sample and not related to bulk absorption changes.[17]

Most pump−probe experiments on OLHPs were conducted with time resolution incapable of recording initial carrier emergence and thermalization. This includes a previous study from this lab which showed that much of the BE PIB appears before substantial cooling of the nascent hot carriers and this was assigned to effects of hot carrier screening on the state density near the BE.[20] The spectral tailing of these screening effects was employed to estimate an exciton binding energy of 20−30 meV for both MAPbI$_3$ and MAPbBr$_3$ layers. But even the improved time resolution employed there did not uncover a signature of exciton dissociation into free carriers. A recent study has addressed these questions using extreme time resolution electronic 2D spectroscopy[21] from which carrier thermalization is concluded to be the fastest process observed, with a duration which is highly dependent on the excitation photon energy. However, the intensity distribution of the pulse

Received: September 6, 2017
Published: November 26, 2017

© 2017 American Chemical Society

DOI: 10.1021/jacs.7b09508
J. Am. Chem. Soc. 2017, 139, 18262−18270

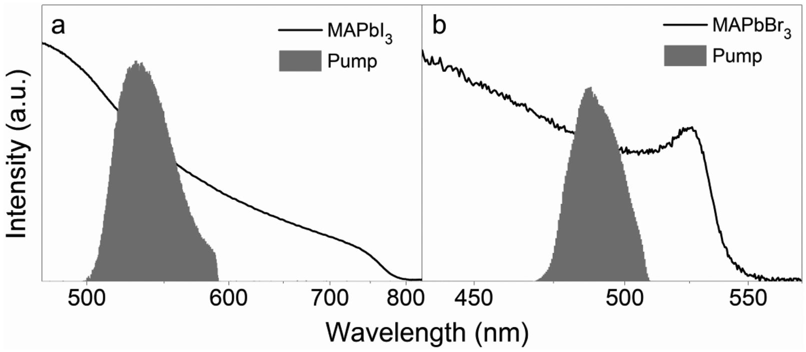

Figure 1. (a) Ground state absorption spectrum of $MAPbI_3$ (black line) and NOPA pump spectrum (gray). (b) Same as (a) for $MAPbBr_3$.

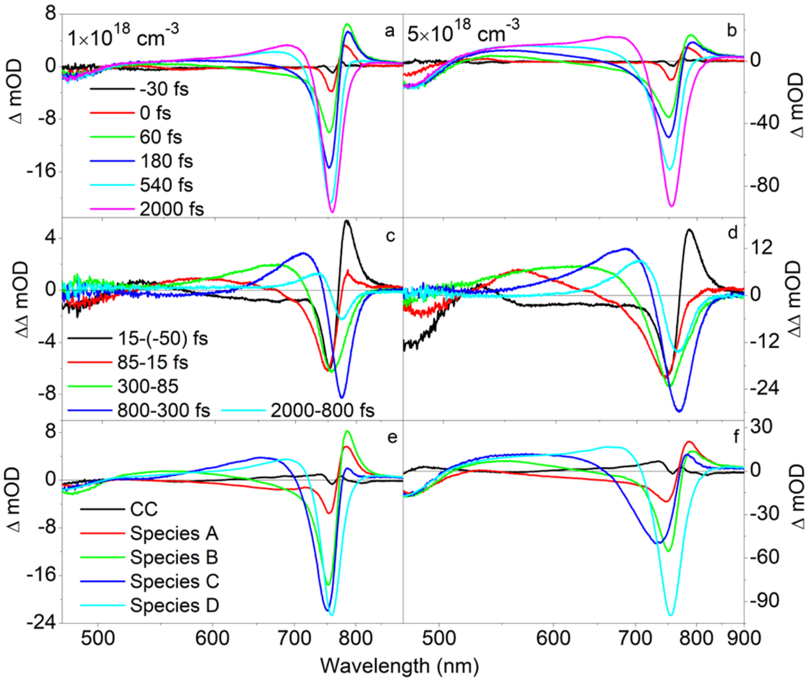

Figure 2. (a, c, e) Transient transmission, finite difference, and species associated spectra of $MAPbI_3$ films after excitation to a carrier density of 1×10^{18} cm^{-3}. (b, d, f) Same for a carrier density of 5×10^{18} cm^{-3}. Associated decay constants for (e) and (f) are presented in Table 1.

spectrum did not allow coverage of the band edge features, which are both highly structured and exhibit much of the early evolution of interest. In particular two of the three features common to ultrafast studies of OLHPs involve this transition explicitly. Thus, despite the extreme time resolution, the results of this experiment do not provide a full spectral mapping which can conclusively analyze such high time resolution experiments in terms of the carrier dynamics they reflect.

There is another material response which is expected to affect spectral evolution of the exciton transition at early times which has strangely not been observed in pump−probe experiments to date, and that is the excitation and relaxation of optical phonons. The importance of optic phonon coupling to the conduction of free carriers in these materials has been extensively discussed in recent publications.[22−31] While the magnitude of electron phonon coupling in OHLPs has been tested by following the temperature dependence of emission line shapes, few time domain measurements have reported impulsive phonon activity like that observed here, and those few have not converged in terms of the active phonon frequencies or their damping dynamics.[32,33]

Here we report a sub-10 fs pump−probe study of microstructured $MAPbI_3$ and $MAPbBr_3$ films. Data analysis proves that sample bleaching rises abruptly with an ∼20 fs delay following photoexcitation which is assigned to dissociation of localized and correlated hot electron hole pairs. The overall bleaching of exciton and interband absorption later rises exponentially by a factor of 2.5 with a 250 fs lifetime, tentatively assigned to increased state filling of the BE exciton during carrier cooling. Spectral modulations in pump−probe signal due to impulsively excited LO phonons are recorded and used to estimate the strength of electron-optic phonon coupling in both materials. The resulting coupling strengths are well within the weak regime and compatible with conduction electrons existing as large polarons.

■ MATERIALS AND METHODS

Thin films of methylammonium lead-halide perovskites were prepared according to a previously described method.[34] In brief, first spin coating of 1 M solutions of PbX_2 (X: I and Br) in dimethylformamide (Sigma-Aldrich) was carried out on 0.5 mm thick glass substrates. The spin velocity was 6500 rpm and the spin-coating duration was 5 s. After the spin-coating, the substrates were annealed at 80 °C for 10

DOI: 10.1021/jacs.7b09508
J. Am. Chem. Soc. 2017, 139, 18262−18270

min. In the second step, the spin coated PbX_2 films were dipped into a solution of 63 mM CH_3NH_3X (X: I and Br) in isopropanol. Following the dipping step, the samples were annealed at 80 °C for another 30 min. The samples were characterized by steady state absorption and photoluminescence spectroscopy. The visible absorption spectra were measured using a Jasco V-670 spectrophotometer and photoluminescence measurements were carried using a fluorescence spectrometer (Edinburgh Instruments FLS920) equipped with a film holder. The pump−probe experiments were performed with a home-built amplified Ti-sapphire laser producing 1 mJ 30 fs pulses centered at 790 nm, at repetition rate of 1 kHz. The amplified output was split in two parts for the generation of the pump and probe, respectively. Sub-10 fs pump pulses were generated in a noncollinear optical parametric amplifier (NOPA) centered either at ∼530 nm (for $MAPbI_3$ experiments) or ∼490 nm (for $MAPbBr_3$ experiments) as shown in Figure 1. The pump was compressed to within 15% of the transform limit using a prism pair (BK7), followed by an aluminum coated deformable mirror. Supercontinuum probe pulses were generated by focusing the 1400 nm output of an optical parametric amplifier (TOPAS 800, Light Conversion) on 2 mm of BaF_2 (in the case of $MAPbI_3$ experiments), or by focusing a 800 nm beam on an ∼2 mm sapphire disk (for $MAPbBr_3$ experiments). Thereafter, the pump and the probe were directed toward the sample using reflective optics. The carrier density dependent experiments were performed by changing the pump fluence. Figure 1 illustrates absorption spectra of the perovskite samples, along with the corresponding pump spectra used for the photoexcitation. The carrier densities immediately after excitation (n_0) were calculated for $MAPbI_3$ as described in the Supporting Information.

■ RESULTS

Pump−probe spectra of $MAPbI_3$ upon NOPA photoexcitation are shown in Figure 2 for two carrier densities (see Figure S1 in the Supporting Information for an additional intermediate density) along with sample and excitation pulse spectra. The general trends described in the introduction are apparent in both. The immediate response of photoexcitation is a red-shift of the absorption with partial bleach at the BE. Over the next ∼1−2 ps, this red-shifted absorption diminishes and at the same time a net bleach builds up at the BE. To isolate various stages of spectral evolution, finite difference spectra are calculated according to eq 1 and presented in the second row of Figure 2.

$$\Delta\Delta\text{OD}(\lambda, t, \Delta t) \equiv \Delta\text{OD}\left(\lambda, t + \frac{\Delta t}{2}\right) - \Delta\text{OD}\left(\lambda, t - \frac{\Delta t}{2}\right) \qquad (1)$$

Noteworthy aspects of the finite difference spectra are (a) upon absorption at both intensities a zero integral peak shift rises sharply at the band edge, and surrounding the second absorption band at 480 nm. (b) An ultrafast buildup of bleaching throughout the interband continuum, peaking at the BE, follows. This bleach red-shifts and narrows over ∼200 fs, erasing the feature described in (a), changes which are assigned to carrier cooling. (c) Concomitant transmission changes surrounding the 480 nm peak differ in that no evolution in this feature is apparent over the carrier cooling stage. Furthermore, its intensity and shape are nonlinearly dependent on the pump fluence. (d) The shifting described in (b) reveals an underlying reduction in transmission over the range from 550 to 650 nm. (e) All spectral features broaden as the excitation intensity is increased.

In order to characterize the spectral evolution in the 480−900 nm range, global kinetic analysis was conducted according to the following kinetic scheme: $\xrightarrow{h\nu} A \xrightarrow{\tau_1} B \xrightarrow{\tau_2} C \xrightarrow{\tau_3} D$, leading to the evolution associated spectra shown in the bottom row of Figure 2. Proper curve fitting required a minimum of five components; an instantaneous coherent coupling contribution (CC in bottom row of Figure 2, not included in the kinetic scheme above), followed by a sequence of four intermediates, all convoluted with a 15 fs Gaussian instrument response function. This kinetic model provided near perfect fits to the low noise data (Figure S2 in the Supporting Information), and resulted in the time constants presented in Table 1.

Table 1. Decay Time Constants for Transitions between the Species Associated Spectra Presented in Figure 2e and f

carrier density, cm^{-3}	τ_1, fs	τ_2, fs	τ_3, fs
1×10^{18}	135 ± 15	180 ± 10	270 ± 15
2.4×10^{18}	120 ± 10	220 ± 10	285 ± 15
5×10^{18}	90 ± 10	285 ± 10	320 ± 15

Inspection of the data closely reveals faint intensity modulations with periods of 100−200 fs. These are assigned to coherent wave packets in optical phonons due to their coupling to the electronic transition. To test the generality of this observation, similar experiments were conducted on $MAPbBr_3$ thin films exciting just above the BE (Figure 3). This also served to test if, as observed in CdSe nanocrystals, coherent phonon modulations become stronger as excitation photon energy approaches the fundamental gap.[35] The modulations were extracted by subtracting a background from the decay components at all probe wavelengths (Figure 4c and

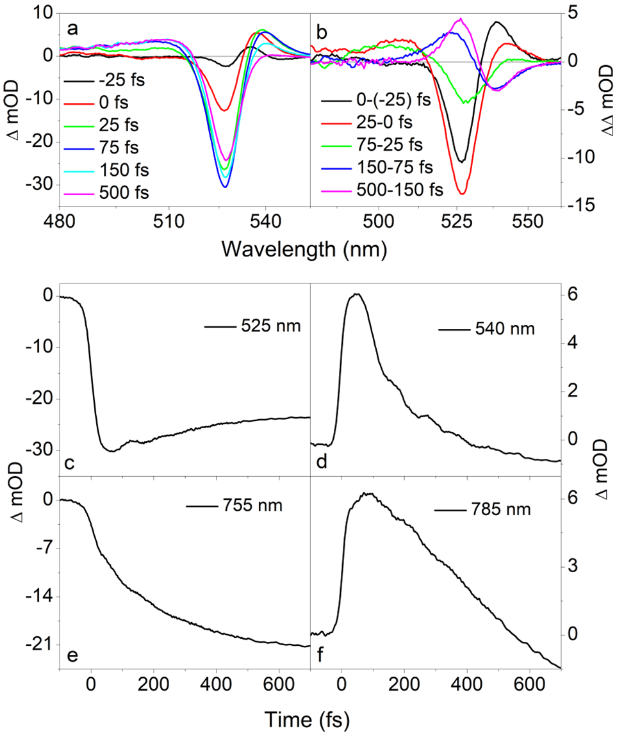

Figure 3. (a) Transient difference and (b) finite difference transmission spectra of $MAPbBr_3$ films after photoexcitation with 490 nm NOPA pulses. (c, d) Temporal changes at the BE bleach and below BE PIA for $MAPbBr_3$ and (e, f) temporal changes at the BE bleach and below BE PIA for $MAPbI_3$ films.

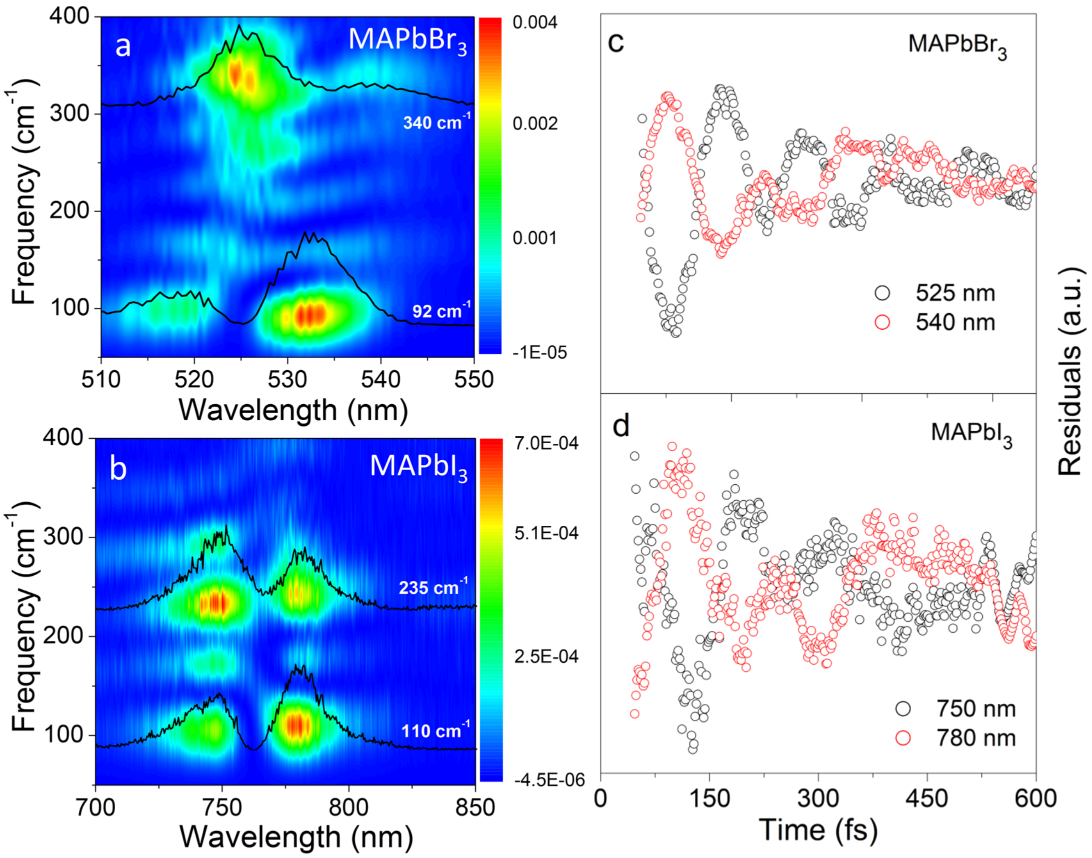

Figure 4. (a, b) Two dimensional map of Fourier power for MAPbBr$_3$ and MAPbI$_3$ films. The abscissa depicts dispersed probe wavelength, while the ordinate indicates the Fourier frequency. The Fourier power is color coded according to the rulers to the right of each panel. Black lines show the power as a function of probe wavelength for the two prominent modulation peaks. (c, d) Residual modulations showing a π-phase shift when probed at two different wavelengths for high frequency modes in MAPbBr$_3$ and in MAPbI$_3$.

d). Fourier analysis was performed to obtain the frequencies of the associated phonons. The left panel in Figure 4 presents the results in color coded maps. Overlaid are cuts which present the power as a function of the probe frequency for both prominent optic phonon peaks observed, at 90 ± 10 and 340 ± 15 cm^{-1} for MAPbBr$_3$, and at 110 ± 10 and 235 ± 15 cm^{-1} for MAPbI$_3$. The low frequency band is tentatively assigned to displacements in the lead-halide scaffolding, while the higher frequencies to motions in the methylammonium ions.[36−38] In both cases, the Fourier mapping shows a doubled peak structure along the probe wavelength axis with humps lying to either side of the exciton peaks in both materials, exhibiting varying degrees of symmetry.

■ DISCUSSION

Two novel facets of OLHP photophysics have been uncovered here. One is the detection of new vibrational modes which modulate the transient transmission spectra. From the modulation depth of the change in probe transmission, coupling strengths to the exciton transition have been estimated. This discovery did not depend on high time resolution, but was facilitated by improved S/N in the pump−probe experiments. A significant characterization and analysis of this finding stems from the recent interest in the impact of lattice deformations on charge mobility and decay dynamics in these materials. Any new input to assess these effects should prove valuable.

The second facet is the discovery of a brief initial state of the excited sample, less than 20 fs in duration, which precedes any phase of absorption bleaching despite excitation high above the ~1.65 eV band edge. Assignment of this phase to the break up of localized carrier pairs is based on its briefness and on the sudden buildup of sample bleach which followes it. This observation is novel not only to experiments on OLHPs, but to bulk semiconductors in general, making the interpretation of its spectral fingerprint a challenge as shown bellow.

Emergence of Hot Carriers in MAPbI$_3$. One objective here was to reveal previously unrecorded early stages of carrier generation in OLHP films. In order to achieve this, laser pulses shorter than 10 fs have been applied in these experiments. The phase of spectral evolution unique to this study can be identified in two measures, species "A" in the kinetic analysis (bottom row of Figure 2) or, equivalently, the black ΔΔOD spectra (middle row of Figure 2). Both spectra consist of sharp peak shift signatures at the edges of both bands. In the finite difference spectra, a similar peak shift signature appears in the 480 nm band as well. According to the global kinetic scheme and its associated rates, this signature rises instantaneously and decays within ~100 fs. However, despite the high quality of fitting provided by the global analysis, similarity of decay times associated with consecutive transitions, as well as deviations at very early delays, demonstrate that a kinetic scenario with distinct species and exponential decays does not capture the underlying dynamics of this system. These results are presented nonetheless to comment on its limitations in light of the

DOI: 10.1021/jacs.7b09508
J. Am. Chem. Soc. 2017, 139, 18262−18270

numerous application of this method in previous studies. Our interpretation will therefore concentrate primarily on the finite difference spectra and spectral band integrals to be described below.

The newly revealed spectral snapshot should be interpreted in context with the established chronology of hot carrier dynamics in bulk semiconductors, starting with exciton dephasing and sub-100 fs thermalization of holes and conduction electrons whose initial energy is dictated by the pump spectrum and carrier effective masses,[39−42,10] followed by picosecond cooling to the lattice temperature through phonon scattering. Sharp peak shifting in ultrafast transient spectra is often related to nonlinear coupling of pump and probe during their temporal overlap, or until the pump induced transition dipoles have dephased. We can exclude this assignment in the present data since these shifts decay only on much longer time scales. To demonstrate this, Figure S3 in the Supporting Information presents a series of finite difference spectra where ΔOD (t = 15 fs) is subtracted from a series of later transient spectra extending up to 100 fs. These are depicted along with the 15 fs transient transmission spectrum. Clearly the ultrafast shift does not decay away over the first tens of femtoseconds as expected from electronic coherent coupling. This ultrafast spectral shifting seemingly precedes thermalization since spectral variations during carrier cooling should be gradual. In contrast, shifts in difference spectra over the initial ∼100 fs of delay shown by species "B" or by the red ΔΔOD curves, reveal a sudden shift to net bleaching. These are assigned to state filling, consistent with the establishment of a hot Fermi−Dirac carrier distribution.

The sharp red-shift at the band edge can be assigned to a shift in exciton and not interband transitions. Stokes shifting of a step-function-like interband absorption would induce absorption below the edge without a concomitant induced transparency above, contrary to the observed trend. Furthermore, an integral of the shift feature near 750 nm is centered at and of the same spectral width of the exciton band (Figure S4 in the Supporting Information) as isolated by modeling of $MAPbI_3$ linear absorption spectra in numerous publications.[12,18] The remarkably good match supports the above assignment.

In order to distinguish between exciton dissociation to carrier thermalization, and demonstrate the delayed nature of the bleach buildup, difference dipole strength band integrals were extracted from the data covering the range from 550 to 900 nm (Figure 5) according to eq 2:

$$\Delta D(t) \equiv \int_{550}^{900} \frac{\Delta \mathrm{OD}(\nu, t)}{\nu}\, \mathrm{d}\nu \tag{2}$$

This measure can detect the onset and evolution of state filling without reference to specific structure in the transient spectrum. The lower cutoff at 550 nm provides selective detection of excitation effects on sample absorption across the fundamental gap without interference from higher transitions. Remarkably, despite significant pump intensity dependence of the TA data in Figures 2a,b, 3e,f, S1 and S5 (Supporting Information) the time dependence of these band integrals is identical within error for all three pump fluences (Figure S6 in the Supporting Information). It consists of an abrupt rise followed by a gradual growth in the net bleach by a factor of 2.5 which is well fit by an exponential of τ = 240 fs.

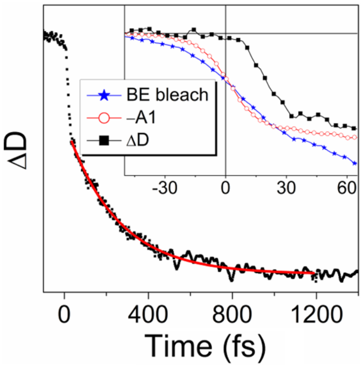

Figure 5. Plot of band integrals for $MAPbI_3$ from 550 to 900 nm calculated according to eq 2. Exponential fit to the delayed rise is overlaid in red. Inset shows initial 60 fs alongside the rises of the below band edge PIA (A1) and BE bleach signals during the same period.

Instead of rising instantly, the sudden onset in bleach is delayed by nearly 20 fs relative to time zero, defined as temporal overlap of pump and probe. This can be seen when comparing the rise in ΔD with that of both halves of the BE shift feature, included in the inset to Figure 5. In bulk semiconductors carrier thermalization has been determined to take place on similar time scales.[39−42] However, since the pump spectrum overlaps significantly with the integration range of ΔD, state filling should be present instantly. Accordingly, the delayed ultrafast appearance of band bleaching is assigned to the emergence of uncorrelated free carriers through exciton dephasing and dissociation. This roughly equals twice the time it takes nascent carriers to separate a distance equal to the average spacing between the photogenerated pairs at the densities tested. This delay is also on par with the dephasing times determined using 2D spectroscopy,[21] suggesting exciton dissociation is the main mechanism of decoherence high above the BG. This appearance time is much shorter than that reported from broadband THz probing studies.[43] Observing this phase hinges on the unique capability of the ultrashort pump pulses to generate localized e−h pairs even high above the BG due to coherent excitation of a broad band of "k" states. The source of delay in bleach appearance while electrons and holes are correlated will require further investigation. It may be due to the crossed polarization of pump and probe chosen to suppress scattering. However, previous photoselective pump−probe experiments on perovskites exhibited very limited effects at later stages of evolution.[14]

Understanding the spectral signature of the dissociating pairs is difficult since very few equivalent studies have been conducted in ordinary inorganic semiconductor solids. Much of the ultrafast study of carrier dynamics in bulk semiconductors from the 1980s and 1990s were conducted by pioneers of ultrafast spectroscopy before advent of the tools we have at our disposal, limiting time resolution by a factor of 2−4, and excluding the flexibility of tuning both of pump and of probe. Nonetheless, the ground-breaking efforts to resolve the earliest stages of free carrier generation by Hu et al.[44] and Bar-Ad and Chemla[45] concur with our assignments. Hu et al. identify an instantaneous polarization of the electron hole pairs even before they have time to separate using THz probing, and assign a characteristic time scale of ∼10 fs. This is in GaAs where the binding energy is minute and this stage should accordingly be shorter than in the OLHP materials. Chemla and Bar-Ad applied an approach similar to our own but limitation of probe bandwidth and pulse durations did not allow full coverage of the band edge exciton peak fully. It would seem however that a fast peak-shift is the leading material response there as well, similar to our own.

Aside from a firm assignment of the earliest spectral shifting to the exciton band, interpretation of its origin, and why it persists well beyond the stage which we assign to dissociation will require identifying whether this feature is related to changes in absorption or in reflection. Possible mechanistic connection between the peak shift observed at early times to a similar feature observed in reflectivity changes in electro-absorption experiments[46−48] will have to await such an identification as well. It is possible that the enhanced polarizability of the excited pairs causes an effective rise in sample dielectric constant providing attractive biexciton interaction lowering the resonance frequency of further exciton absorption. The slow decay of this feature may indicate that such stabilization can also be affected by carriers which have lost correlation as well. In any case, it makes perfect sense that state filling effects kick in only once the nascent pair coherences dephase and populations are established.

The next stage of spectral evolution complete in roughly 100 fs is assigned to establishment of a thermal distribution of hot carriers. This delay is longer than reported for some inorganic semiconductors. The only experiment conducted with similar time resolution on this material employing 2D spectroscopy[21] extracted pump wavelength dependent thermalization times in the 10−50 fs range, in fair agreement with observations here.

Cooling of Hot Carriers. Later stages of spectral evolution consist of a gradual shift to the blue and a narrowing of the bleach from shorter to longer probe wavelengths. This shift uncovers an underlying net reduction in transmission in the range from 510 to 730 nm, assignment of which is the subject of debate.[17,18] Deschler and co-workers, who separately measured transient transmission and reflection, have attributed this to pump induced changes in reflectivity.[17] Yang et al. who also measured reflectivity effects, concluded instead that BG renormalization is responsible to this broad PIA.[18] A recent report by Anand et al. assign the broad induced absorption to the presence of additional valence and/or conduction bands.[49] Since reflectivity was not addressed here, we cannot contribute to this debate. The trend of continuous red-shifting and narrowing of a bleach toward the BE is in line with cooling induced concentration of the photoinduced carriers at the bottom of the conduction and valence bands.[15−18,20]

One noteworthy aspect concerns the near linearity of the amplitude of post cooling transient spectra with pump fluence as demonstrated in Figure S7 in the Supporting Information. This proves that within the range of carrier densities experimented with here, population of the exciton states remains limited, without significant Burstein−Moss shifting. This is surprising since densities here approach one excitation per Bohr volume. Even with significant thermal dissociation of excitons at room temperature, transient spectra should exhibit some saturation of the band edge bleach. This, however, depends on the exciton binding energy, estimates of which vary widely.[46,50,51]

Another aspect is the disappearance of the exciton state peak shift as carrier cooling advances at all three excitation densities. This feature is present for at least 100 fs after rising abruptly and is assigned to screening effects on the excitonic peak. Why this shift decays during cooling cannot be explained by complete state filling of the exciton band since even at the highest pump fluence the combined losses due to changes in absorption and reflection are a small fraction of the sample OD. We note that a similar decay in biexciton shifting at the band edge is also observed in pump−probe experiments on semiconductor nanocrystals.[52−54]

Comparison of transmission changes surrounding the fundamental band edge with the 480 nm peak shows that the ratio of intensities of these signatures decreases markedly with increasing pump fluence. The latter which is nearly unobservable at the lowest pump intensity becomes half as strong at the higher fluence as the shift band around 750 nm. Interpreting this requires a separation of pump induced changes in transmission and reflection with the current time resolution and spectral coverage. Furthermore, the 480 nm band is curiously unaffected by carrier cooling at either pump intensity in contrast to the significant transmission changes near 750 nm. This points to asymmetry in the dynamics of carrier cooling between the conduction and valence bands, only one of which is suggested to be mutual to both transitions.[55] This is unexpected since effective masses are similar in conduction and valence bands.

The gradual rise exhibited by ΔD over hundreds of femtoseconds requires further comment. Modeling of band filling effects is usually performed assuming independence of the transition dipole on $\vec{k}$, producing interband absorption which is linear in the joint density of states.[18] If this approach were rigorous and absorption bleaching was due exclusively to blocking of interband transitions, the integrated bleach would be constant. This strong deviation may reflect a combination of three possible factors. On the one hand, the assumption of independence of mVC on either may be incorrect. Another possibility is that the enhanced apparent bleach is due to the buildup of stimulated emission which appears once carriers in both bands have relaxed to the band edge. The third involves the effects of an increasing population and blocking of absorption to the $n = 1$ exciton band which accompanies carrier cooling.[51] In any case, this observation questions interpretations of pump−probe data in terms of bleach conserving models for extracting the time dependence of carrier temperatures.

Electron−Phonon Coupling in $MAPbBr_3$ and $MAPbI_3$ Films. Nascent free carriers also couple to optical phonons via the Fröhlich mechanism which has recently been investigated by many groups.[22−27,32,33,56−58] All subsequent dynamical processes, including mobility and recombination, are influenced by the strength of this interaction, making its quantification essential. In this section, we will focus on the signatures of coherent underdamped optical phonons on our measurements and how it can serve to estimate the coupling strength to these modes. In the pump−probe data, we observed spectral modulations surrounding the band edge both in $MAPbBr_3$ and $MAPbI_3$ due to electron−phonon coupling. The periodic modulations in the residuals were obtained by subtracting a background from the transient kinetics (Figure 4c and d). Fourier analysis of the residuals identifies frequencies of the phonons and the intensity of modulation at various probe wavelengths.

For $MAPbBr_3$, the phonon frequencies are 90 ± 10 and 340 ± 15 cm^{-1} (Figure 4a). The low frequency band has been assigned to optical phonons involving the lead−halide scaffolding, and the higher frequencies to motions in the methylammonium ion.[36−38] The two clearly observed phonon frequencies in $MAPbI_3$ are 110 ± 10 and 235 ± 15 cm^{-1} (Figure 4b). In both cases faint additional peaks are observed between these prominent features, whose identity is the subject

DOI: 10.1021/jacs.7b09508
J. Am. Chem. Soc. 2017, 139, 18262−18270

of ongoing study. Furthermore, exciting $MAPbI_3$ at the band gap showed similar modulation amplitudes as excitation high above it, as presented in Figure S8 in the Supporting Information, contrary to observations in semiconductor nanocrystals.[35]

The identity of the high frequency mode previously assigned to torsions of the MA cation is subject to some debate. The large shift of this mode for different halide perovskite has been suggested to reflect strong interaction between the PbX_3^- and $CH_3NH_3^+$ resulting in a restricted rotation of the methyl around its C−N axis.[59] However, a recent study has suggested that this mode is no longer valid for the MA cation torsion since it show up the Raman spectra of both $MAPbBr_3$ and $CsPbBr_3$ perovskites.[60] As for the low frequency modulations observed in the two samples, that observed for the bromide falls below that in the iodide. There is nothing in our experiments which can explain this puzzling result. Either this mode involves negligible motion of the halide, or is fundamentally different in the two materials. Answering this will require further investigation.

Impulsive excitation of molecular chromophores induced coherent vibrations in the excited state by simultaneous population of numerous vibronic levels in the form of a localized wave packet, and in the ground state via impulsive resonance Raman scattering. As shown in Figure 4a, the modulation amplitudes peak in two lobes on either side of the bromide exciton peak, with 1π phase shift on either side (Figure 4c and d). This indicates that the effect of the vibration is primarily to shift the central wavelength of the exciton transition. In molecules, excited state and ground state populations are distinct, a separation which is more difficult in solids where our understanding is based on delocalized excitations. Rather than untangling this distinction here, a heuristic analysis similar to that described for quantum dots by Kambhampati and co-workers is applied.[35]

A displaced harmonic oscillator model for the band edge exciton transition is envisioned, with the depth of modulation obtained by comparing the modulation amplitudes to that of the bleach itself. Electron−phonon coupling strengths are represented by a set of parameters $[\Delta, S, \lambda]$. Δ is a dimensionless displacement of the normal coordinate, S is the Huang−Rhys parameter, and λ is the reorganization energy. S is related to Δ as $S = \Delta^2/2$, and the reorganization energy λ to S as $\lambda = \hbar\omega_{LO}S$, where ω_{LO} is the frequency of the optical phonon. λ $(\hbar\Delta\omega)$ was calculated from our data using $A_{OSC} = \left(\frac{d\,OD}{d\omega}\right)\Delta\omega$, where OD is the optical density of the sample and A_{OSC} is the amplitude of the oscillations in the same units. $d\,OD/d\omega$ was obtained from excitonic absorption spectra from the literature normalized to 20 mOD for $MAPbI_3$ and 30 mOD for $MAPbBr_3$ (amplitude of the band edge bleach in our data).[18,61] $\frac{d\,OD}{d\omega}$ was obtained by numerical differentiation. A_{OSC} of the high frequency modes (~340 and ~235 cm^{-1}) was obtained by fitting the residuals to a damped sine function which was then extrapolated to $t = 0$. Amplitudes of the low frequency modes were estimated directly from the scans. The resulting coupling strengths, displacements and reorganization energies for both materials and modes are provided in the Table 2. Since $S < 1$ in both materials, weak electron−phonon coupling of the detected underdamped modes predicting formation of large polarons in both materials.

Table 2. Electron−Phonon Coupling Parameters Determined for $MAPbI_3$ and $MAPbBr_3$

	$\hbar\omega_{LO}$ (meV)	S	Δ	λ (meV)
$MAPbI_3$	29.13	0.04	0.3	1.1
	13.63	0.02	0.2	0.3
$MAPbBr_3$	42.15	0.08	0.4	3.5
	11.4	0.09	0.4	1.1

These results join those of a growing number of studies addressing OLHP electron phonon coupling, whose findings have yet to converge in terms of frequencies, coupling strengths, and mode dynamics. The interest in this aspect of OLHP photophysics stems from the realization that despite the predominant involvement of the inorganic framework in defining their electronic structure, carrier mobilities fall midway between those observed in conventional inorganic semiconductors and in organic conductors. Other underdamped modes likewise revealed through impulsive spectroscopy vary in frequency from tens to several hundred wavenumbers, while frequency domain spectroscopies highlight modes in the 10−50 cm^{-1} range which are predominantly overdamped at room temperature.[57] Full comprehension of the role played by all these vibrations in any particular photophysical attribute of OLHP films will require consolidation of these findings.[23,25,32,62] Toward establishing such consolidation it is of utmost importance that all empirical findings concerning frequencies and coupling strengths of active modes be reported in the literature. Nonetheless, assuming the moderate charge mobilities in OLHPs has been correctly assigned to intermediate electron phonon coupling, the modes reported here would appear not to be responsible for this effect.

■ CONCLUSION

High signal-to-noise pump−probe measurements with sub-10 fs pulses were performed to uncover early stages of carrier dynamics and electron-optic phonon coupling in lead halide perovskite films. Immediately after photoexcitation, localized hot excitons are generated which exhibit a sharp red-shift of the excitonic peak in the TA spectra. These localized hot excitons then dissociate to free carriers with a time scale ~20 fs followed by thermalization which is complete within 100 fs as evidenced in band integrals and global kinetic analysis. Later, hot carriers cool to lattice temperature through scattering with optic phonons within 0.5 ps. The charge carriers also couple to the optic phonons which result in spectral modulations surrounding the band edge in both the materials. Fourier analysis of these modulations shows active phonons with frequency ~ 100 cm^{-1} related to stretching modes of Pb-halide moieties and in the 250−350 cm^{-1} range previously assigned to torsional motion of the methylammonium cation. The amplitudes of these modulations allowed estimates for the underlying electron phonon coupling strengths showing all to be well within the weak regime and compatible for large polaron formation in these materials, and thus probably not responsible to the moderate carrier mobilities in these materials.

■ ASSOCIATED CONTENT

Ⓢ Supporting Information

The Supporting Information is available free of charge on the ACS Publications website at DOI: 10.1021/jacs.7b09508.

Estimation of carrier density, fitting of TA data using Global kinetic analysis model and other spectroscopic data (PDF)

AUTHOR INFORMATION

Corresponding Author

*sandy@mail.huji.ac.il

ORCID

Tufan Ghosh: 0000-0002-4898-2117
Lioz Etgar: 0000-0001-6158-8520
Sanford Ruhman: 0000-0003-0575-1367

Notes

The authors declare no competing financial interest.

ACKNOWLEDGMENTS

S.R. holds the Lester Aronberg Chair in Chemistry. S.R. acknowledges support from the US-Israel Binational Science foundation and the Israel Science Foundation. S.R. thanks Prof. M. Bonn, S. Koch, L. Kronik, R. Baer and doctors O. Yaffe, J. Ruhman, and B. Skinner for enlightening discussions. T.G. thanks the Lady Davis Fellowship Trust and the Raymond and Janine Bollag Post-Doctoral Fellowship Fund for a fellowship. S.R. and T.G. thank Dr. Oleg Liubashevski for technical assistances. L.E. acknowledges the China-Israel grant under the Israel Ministry of Science.

REFERENCES

(1) Lee, M. M.; Teuscher, J.; Miyasaka, T.; Murakami, T. N.; Snaith, H. J. *Science* **2012**, *338*, 643−647.

(2) Grätzel, M. *Nat. Mater.* **2014**, *13*, 838−842.

(3) Green, M. A.; Ho-Baillie, A.; Snaith, H. J. *Nat. Photonics* **2014**, *8*, 506−514.

(4) Kojima, A.; Teshima, K.; Shirai, Y.; Miyasaka, T. *J. Am. Chem. Soc.* **2009**, *131*, 6050−6051.

(5) Jeon, N. J.; Noh, J. H.; Kim, Y. C.; Yang, W. S.; Ryu, S.; Seok, S. I. *Nat. Mater.* **2014**, *13*, 897−903.

(6) Kim, H.-S.; Lee, C.-R.; Im, J.-H.; Lee, K.-B.; Moehl, T.; Marchioro, A.; Moon, S.-J.; Humphry-Baker, R.; Yum, J.-H.; Moser, J. E.; Grätzel, M.; Park, N. − G. *Sci. Rep.* **2012**, *2*, 591.

(7) Stranks, S. D.; Eperon, G. E.; Grancini, G.; Menelaou, C.; Alcocer, M. J. P.; Leijtens, T.; Herz, L. M.; Petrozza, A.; Snaith, H. J. *Science* **2013**, *342*, 341−344.

(8) Burschka, J.; Pellet, N.; Moon, S.-J.; Humphry-Baker, R.; Gao, P.; Nazeeruddin, M. K.; Grätzel, M. *Nature* **2013**, *499*, 316−319.

(9) Malinkiewicz, O.; Yella, A.; Lee, Y. H.; Espallargas, G. M.; Graetzel, M.; Nazeeruddin, M. K.; Bolink, H. J. *Nat. Photonics* **2014**, *8*, 128−132.

(10) Huang, J.; Yuan, Y.; Shao, Y.; Yan, Y. *Nat. Rev. Mater.* **2017**, *2*, 17042.

(11) He, H.; Yu, Q.; Li, H.; Li, J.; Si, J.; Jin, Y.; Wang, N.; Wang, J.; He, J.; Wang, X.; Zhang, Y.; Ye, Z. *Nat. Commun.* **2016**, *7*, 10896.

(12) Saba, M.; Cadelano, M.; Marongiu, D.; Chen, F.; Sarritzu, V.; Sestu, N.; Figus, C.; Aresti, M.; Piras, R.; Lehmann, A. G.; Cannas, C.; Musinu, A.; Quochi, F.; Mura, A.; Bongiovanni, G. *Nat. Commun.* **2014**, *5*, 5049.

(13) Piatkowski, P.; Cohen, B.; Javier Ramos, F.; Di Nunzio, M.; Nazeeruddin, M. K.; Grätzel, M.; Ahmad, S.; Douhal, A. *Phys. Chem. Chem. Phys.* **2015**, *17*, 14674−14684.

(14) Zhai, Y.; Sheng, C. X.; Zhang, C.; Vardeny, Z. V. *Adv. Funct. Mater.* **2016**, *26*, 1617−1627.

(15) Manser, J. S.; Kamat, P. V. *Nat. Photonics* **2014**, *8*, 737−743.

(16) Trinh, M. T.; Wu, X.; Niesner, D.; Zhu, X.-Y. *J. Mater. Chem. A* **2015**, *3*, 9285−9290.

(17) Price, M. B.; Butkus, J.; Jellicoe, T. C.; Sadhanala, A.; Briane, A.; Halpert, J. E.; Broch, K.; Hodgkiss, J. M.; Friend, R. H.; Deschler, F. *Nat. Commun.* **2015**, *6*, 8420.

(18) Yang, Y.; Ostrowski, D. P.; France, R. M.; Zhu, K.; van de Lagemaat, J.; Luther, J. M.; Beard, M. C. *Nat. Photonics* **2016**, *10*, 53−59.

(19) Chen, K.; Barker, A. J.; Morgan, F. L. C.; Halpert, J. E.; Hodgkiss, J. M. *J. Phys. Chem. Lett.* **2015**, *6*, 153−158.

(20) Sharma, V.; Aharon, S.; Gdor, I.; Yang, C.; Etgar, L.; Ruhman, S. *J. Mater. Chem. A* **2016**, *4*, 3546−3553.

(21) Richter, J. M.; Branchi, F.; Valduga de Almeida Camargo, F.; Zhao, B.; Friend, R. H.; Cerullo, G.; Deschler, F. *Nat. Commun.* **2017**, *8*, 376.

(22) Zhu, H.; Miyata, K.; Fu, Y.; Wang, J.; Joshi, P. P.; Niesner, D.; Williams, K. W.; Jin, S.; Zhu, X.-Y. *Science* **2016**, *353*, 1409−1413.

(23) Wright, A. D.; Verdi, C.; Milot, R. L.; Eperon, G. E.; Pérez-Osorio, M. A.; Snaith, H. J.; Giustino, F.; Johnston, M. B.; Herz, L. M. *Nat. Commun.* **2016**, *7*, 11755.

(24) Straus, D. B.; Hurtado Parra, S.; Iotov, N.; Gebhardt, J.; Rappe, A. M.; Subotnik, J. E.; Kikkawa, J. M.; Kagan, C. R. *J. Am. Chem. Soc.* **2016**, *138*, 13798−13801.

(25) Mante, P.-A.; Stoumpos, C. C.; Kanatzidis, M. G.; Yartsev, A. *Nat. Commun.* **2017**, *8*, 14398.

(26) Sendner, M.; Nayak, P. K.; Egger, D. A.; Beck, S.; Müller, C.; Epding, B.; Kowalsky, W.; Kronik, L.; Snaith, H. J.; Pucci, A.; Lovrinčić, R. *Mater. Horiz.* **2016**, *3*, 613−620.

(27) Monahan, D. M.; Guo, L.; Lin, J.; Dou, L.; Yang, P.; Fleming, G. R. *J. Phys. Chem. Lett.* **2017**, *8*, 3211−3215.

(28) Ivanovska, T.; Dionigi, C.; Mosconi, E.; De Angelis, F.; Liscio, F.; Morandi, V.; Ruani, G. *J. Phys. Chem. Lett.* **2017**, *8*, 3081.

(29) Wolf, C.; Cho, H.; Kim, Y.-H.; Lee, T.-W. *ChemSusChem* **2017**, *10*, 3705.

(30) Karakus, M.; Jensen, S. A.; D'Angelo, F.; Turchinovich, D.; Bonn, M.; Cánovas, E. *J. Phys. Chem. Lett.* **2015**, *6*, 4991.

(31) Bonn, M.; Miyata, K.; Hendry, E.; Zhu, X.-Y. *ACS Energy Lett.* **2017**, *2*, 2555.

(32) Batignani, G.; Fumero, G.; Kandada, A. R. S.; Cerullo, G.; Gandini, M.; Ferrante, C.; Petrozza, A.; Scopigno, T. arXiv:1705.08687, **2017**.

(33) Miyata, K.; Meggiolaro, D.; Trinh, M. T.; Joshi, P. P.; Mosconi, E.; Jones, S. C.; De Angelis, F.; Zhu, X.-Y. *Sci. Adv.* **2017**, *3*, e1701217.

(34) Aharon, S.; Cohen, B. E.; Etgar, L. *J. Phys. Chem. C* **2014**, *118*, 17160−17165.

(35) Sagar, D. M.; Cooney, R. R.; Sewall, S. L.; Dias, E. A.; Barsan, M. M.; Butler, I. S.; Kambhampati, P. *Phys. Rev. B: Condens. Matter Mater. Phys.* **2008**, *77*, 235321.

(36) Quarti, C.; Grancini, G.; Mosconi, E.; Bruno, P.; Ball, J. M.; Lee, M. M.; Snaith, H. J.; Petrozza, A.; Angelis, F. D. *J. Phys. Chem. Lett.* **2014**, *5*, 279−284.

(37) Niemann, R. G.; Kontos, A. G.; Palles, D.; Kamitsos, E. I.; Kaltzoglou, A.; Brivio, F.; Falaras, P.; Cameron, P. J. *J. Phys. Chem. C* **2016**, *120*, 2509−2519.

(38) Pistor, P.; Ruiz, A.; Cabot, A.; Izquierdo-Roca, V. *Sci. Rep.* **2016**, *6*, 35973.

(39) Rota, L.; Lugli, P.; Elsaesser, T.; Shah, J. *Phys. Rev. B: Condens. Matter Mater. Phys.* **1993**, *47*, 4226−4237.

(40) Hunsche, S.; Heesel, H.; Ewertz, A.; Kurz, H.; Collet, J. H. *Phys. Rev. B: Condens. Matter Mater. Phys.* **1993**, *48*, 17818−17826.

(41) Masumoto, Y.; Fluegel, B.; Meissner, K.; Koch, S. W.; Binder, R.; Paul, A.; Peyghambarian, N. *J. Cryst. Growth* **1992**, *117*, 732−737.

(42) Shah, J. *Ultrafast Spectroscopy of Semiconductors and Semiconductor Nanostructures*; Springer Science & Business Media: New York, 2013.

(43) Valverde-Chávez, D. A.; Ponseca, C. S.; Stoumpos, C. C.; Yartsev, A.; Kanatzidis, M. G.; Sundström, V.; Cooke, D. G. *Energy Environ. Sci.* **2015**, *8*, 3700−3707.

(44) Hu, B. B.; de Souza, E. A.; Knox, W. H.; Cunningham, J. E.; Nuss, M. C.; Kuznetsov, A. V.; Chuang, S. L. *Phys. Rev. Lett.* **1995**, *74*, 1689−1692.

(45) Bar-Ad, S.; Chemla, D. S. *Mater. Sci. Eng., B* **1997**, *48*, 83−87.
(46) Ziffer, M. E.; Mohammed, J. C.; Ginger, D. S. *ACS Photonics* **2016**, *3*, 1060−1068.
(47) Roiati, V.; Mosconi, E.; Listorti, A.; Colella, S.; Gigli, G.; De Angelis, F. *Nano Lett.* **2014**, *14*, 2168−2174.
(48) Deschler, F.; Price, M.; Pathak, S.; Klintberg, L. E.; Jarausch, D.-D.; Higler, R.; Hüttner, S.; Leijtens, T.; Stranks, S. D.; Snaith, H. J.; Atatüre, M.; Phillips, R. T.; Friend, R. H. *J. Phys. Chem. Lett.* **2014**, *5*, 1421−1426.
(49) Anand, B.; Sampat, S.; Danilov, E. O.; Peng, W.; Rupich, S. M.; Chabal, Y. J.; Gartstein, Y. N.; Malko, A. V. *Phys. Rev. B: Condens. Matter Mater. Phys.* **2016**, *93*, 161205.
(50) Yang, Z.; Surrente, A.; Galkowski, K.; Bruyant, N.; Maude, D. K.; Haghighirad, A. A.; Snaith, H. J.; Plochocka, P.; Nicholas, R. J. *J. Phys. Chem. Lett.* **2017**, *8*, 1851−1855. Please also see the relevant references in the article.
(51) Sestu, N.; Cadelano, M.; Sarritzu, V.; Chen, F.; Marongiu, D.; Piras, R.; Mainas, M.; Quochi, F.; Saba, M.; Mura, A.; Bongiovanni, G. *J. Phys. Chem. Lett.* **2015**, *6*, 4566−4572.
(52) Klimov, V. I. *J. Phys. Chem. B* **2000**, *104*, 6112−6123.
(53) Gdor, I.; Shapiro, A.; Yang, C.; Yanover, D.; Lifshitz, E.; Ruhman, S. *ACS Nano* **2015**, *9*, 2138−2147.
(54) Sewall, S. L.; Franceschetti, A.; Cooney, R. R.; Zunger, A.; Kambhampati, P. *Phys. Rev. B: Condens. Matter Mater. Phys.* **2009**, *80*, 081310.
(55) Xing, G.; Mathews, N.; Sun, S.; Lim, S. S.; Lam, Y. M.; Grätzel, M.; Mhaisalkar, S.; Sum, T. C. *Science* **2013**, *342*, 344−347.
(56) Filippetti, A.; Mattoni, A.; Caddeo, C.; Saba, M. I.; Delugas, P. *Phys. Chem. Chem. Phys.* **2016**, *18*, 15352−15362.
(57) Yaffe, O.; Guo, Y.; Tan, L. Z.; Egger, D. A.; Hull, T.; Stoumpos, C. C.; Zheng, F.; Heinz, T. F.; Kronik, L.; Kanatzidis, M. G.; Owen, J. S.; Rappe, A. M.; Pimenta, M. A.; Brus, L. E. *Phys. Rev. Lett.* **2017**, *118*, 136001.
(58) Bakulin, A. A.; Selig, O.; Bakker, H. J.; Rezus, Y. L. A.; Müller, C.; Glaser, T.; Lovrincic, R.; Sun, Z.; Chen, Z.; Walsh, A.; Frost, J. M.; Jansen, T. L. C. *J. Phys. Chem. Lett.* **2015**, *6*, 3663−3669.
(59) Xie, L.-Q.; Zhang, T.-Y.; Chen, L.; Guo, N.; Wang, Y.; Liu, G.-K.; Wang, J.-R.; Zhou, J.-Z.; Yan, J.-W.; Zhao, Y.-X.; Mao, B.-W.; Tian, Z.-Q. *Phys. Chem. Chem. Phys.* **2016**, *18*, 18112−18118.
(60) Guo, Y.; Yaffe, O.; Paley, D. W.; Beecher, A. N.; Hull, T. D.; Szpak, G.; Owen, J. S.; Brus, L. E.; Pimenta, M. A. *Phys. Rev. Mater.* **2017**, *1*, 042401.
(61) Kumawat, N. K.; Dey, A.; Kumar, A.; Gopinathan, S. P.; Narasimhan, K. L.; Kabra, D. *ACS Appl. Mater. Interfaces* **2015**, *7*, 13119−13124.
(62) Phuong, L. Q.; Nakaike, Y.; Wakamiya, A.; Kanemitsu, Y. *J. Phys. Chem. Lett.* **2016**, *7*, 4905−4910.

DOI: 10.1021/jacs.7b09508
J. Am. Chem. Soc. 2017, 139, 18262−18270